

Supporting Information

to the paper entitled

Drastic Effect of Lattice Propionitrile Molecules on the Spin-Transition Temperature in a 2,2'-Dipyridylamino/s-Triazine-Based Iron(II) Complex

by

*Nanthawat Nanthawat Wannarit,^{†,‡,◊} Nassim Nassirinia,^{†,§} Saeid Amani,[§] Norberto Masciocchi, *//*

*Sujitra Youngme,[‡] Olivier Roubeau, *⊥ Simon J. Teat[∇] and Patrick Gamez*†,#*

† Departament de Química Inorgànica, Universitat de Barcelona, Martí i Franquès 1-11, 08028
Barcelona, Spain

‡ Materials Chemistry Research Unit, Department of Chemistry and Center of Excellence for
Innovation in Chemistry, Faculty of Science, Khon Kaen University, Khon Kaen 40002, Thailand

§ Arak University, Faculty of Sciences, Department of Chemistry, Arak 38156-8-8349, Iran

// Dipartimento di Scienza e Alta Tecnologia and To.Sca.Lab, Università dell’Insubria, Via
Valleggio 11, 22100 Como, Italy

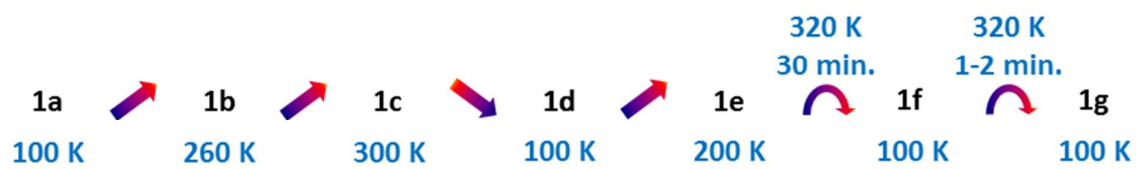
⊥ Instituto de Ciencia de Materiales de Aragón (ICMA), CSIC and Universidad de Zaragoza,
Plaza San Francisco s/n, 50009 Zaragoza, Spain

∇ Advanced Light Source (ALS), Lawrence Berkeley National Laboratory, 1 Cyclotron Road,
Berkeley, CA 94720, USA

Institució Catalana de Recerca i Estudis Avançats (ICREA), Passeig Lluís Companys 23, 08010
Barcelona, Spain

Table of Contents

Scheme S1. Heating/cooling sequence	S2
Table S1. Crystal data and structure refinement for complex $\mathbf{1}^{\text{NCSe}} \cdot \mathbf{2\text{PrCN}}$	S3
Table S2. Coordination bond lengths and angles and supramolecular parameters for $\mathbf{1}^{\text{NCSe}} \cdot \mathbf{2\text{PrCN}}$	S4-S5
Figure S1. DSC traces of fresh and aged $\mathbf{1}^{\text{NCSe}} \cdot \mathbf{2\text{PrCN}}$	S6
Figure S2. χT vs. T plot of successive temperature scans on $\mathbf{1}^{\text{NCSe}} \cdot \mathbf{2\text{PrCN}}$	S7
Figure S3. Thermogravimetric analysis of fresh $\mathbf{1}^{\text{NCSe}} \cdot \mathbf{2\text{PrCN}}$.	S8
Figure S4. infra-red spectra $\mathbf{1}^{\text{NCSe}} \cdot \mathbf{2\text{PrCN}}$ and $\mathbf{1}^{\text{NCSe}}$	S8
Figure S5. Raw powder diffraction data for $\mathbf{1}^{\text{NCSe}}$	S9
Figure S6. Crystal-packing views of $\mathbf{1}^{\text{NCSe}} \cdot \mathbf{2\text{PrCN}}$ showing the location of the lattice propionitrile molecules	S10



Scheme S1. Temperature sequence used for the temperature-dependent X-ray diffraction analysis of one single crystal of $[\text{Fe}(\text{L1}^{\text{F}})_2(\text{NCSe})_2] \cdot 2\text{CH}_3\text{CH}_2\text{CN}$ ($\text{1}^{\text{NCSe}} \cdot \text{2PrCN}$).

Table S1. Crystal data and structure refinement for complex **1^{NCSe}·2PrCN** at different temperatures, following the heating/cooling sequence depicted in Scheme S1.

Compound	1a	1b	1c	1d	1e	1f	1g
Empirical formula	$C_{52}H_{16}F_{20}FeN_{14}O_4Se_2, 2(C_3H_5N)$						
Formula weight (g mol ⁻¹)	1604.72						
Temperature (K)	100(2)	260(2)	300(2)	100(2)	200(2)	100(2)	100(2)
Crystal system	triclinic						
Space group	<i>P</i> -1						
Crystal size (mm ³)	0.30 × 0.02 × 0.02						
<i>a</i> (Å)	8.4681(7)	8.638(2)	8.807(1)	8.484(1)	8.562(1)	8.489(1)	8.492(2)
<i>b</i> (Å)	11.361(1)	11.490(3)	11.501(2)	11.378(2)	11.457(1)	11.386(2)	11.405(2)
<i>c</i> (Å)	15.875(1)	15.947(4)	16.021(3)	15.878(2)	15.917(1)	15.873(2)	15.866(3)
α (°)	92.253(2)	93.348(3)	93.578(2)	92.450(2)	93.176(2)	92.602(2)	92.806(2)
β (°)	100.471(2)	100.538(3)	100.055(2)	100.385(2)	100.511(2)	100.313(2)	100.195(3)
γ (°)	99.070(2)	100.730(3)	101.647(2)	99.220(2)	100.139(2)	99.320(2)	99.416(3)
<i>V</i> (Å ³)	1479.5(2)	1521.8(7)	1556.9(5)	1484.0(4)	1504.9(2)	1485.1(4)	1487.1(5)
<i>Z</i>	1						
ρ_{calcd}	1.801	1.751	1.711	1.796	1.771	1.794	1.792
μ (mm ⁻¹)	2.005	1.949	1.905	1.998	1.971	1.997	1.994
<i>F</i> (000)	792						
ϑ for data collection (°)	3.07–33.54	3.16–27.30	3.11–25.56	3.06–28.30	3.02–29.88	2.80–31.05	3.05–30.92
Reflections collected / unique	43083 / 8981	13217 / 6619	10848 / 5096	33128 / 6085	31873 / 6878	32392 / 7054	23224 / 7049
Completeness to theta	99.2	98.3	99.0	99.8	99.6	99.7	99.5
Data / restraints / parameters	8981 / 0 / 458	6619 / 0 / 458	5096 / 7 / 458	6085 / 0 / 458	6878 / 0 / 458	7054 / 0 / 458	7049 / 0 / 458
Goodness-of-fit on <i>F</i> ²	1.020	0.967	0.969	1.027	1.034	1.043	1.040
Final R indices [$>2\sigma(I)$]	R1 = 0.0361, wR2 = 0.0937	R1 = 0.0612, wR2 = 0.1803	R1 = 0.0593, wR2 = 0.1734	R1 = 0.0415, wR2 = 0.1032	R1 = 0.0404, wR2 = 0.1055	R1 = 0.0425, wR2 = 0.1121	R1 = 0.0507, wR2 = 0.1344
R indices (all data)	R1 = 0.0444, wR2 = 0.0989	R1 = 0.0793, wR2 = 0.1967	R1 = 0.0766, wR2 = 0.1890	R1 = 0.0553, wR2 = 0.1111	R1 = 0.0519, wR2 = 0.1130	R1 = 0.0588, wR2 = 0.1205	R1 = 0.0755, wR2 = 0.1478
largest diff. peak and hole (e Å ³)	0.617 and -0.728	0.470 and -0.692	0.521 and -0.540	0.679 and -0.812	0.304 and -0.566	0.771 and -0.886	0.747 and -1.008

Table S2. Coordination bond lengths (\AA) and angles ($^\circ$), and supramolecular interactions for compound $\mathbf{1}^{\text{NCSe}}\cdot\mathbf{2}\text{PrCN}^a$ at different temperatures, following the heating/cooling sequence depicted in Scheme S1.

Compound	1a	1b	1c	1d	1e	1f	1g
<i>Bond</i>	100(2)	260(2)	300(2)	100(2)	200(2)	100(2)	100(2)
Fe1–N1	1.930(1)	1.948(3)	2.037(5)	1.929(2)	1.937(2)	1.936(2)	1.937(3)
Fe1–N2	1.981(1)	2.011(3)	2.161(3)	1.984(2)	1.986(2)	1.983(2)	1.989(2)
Fe1–N3	1.979(1)	2.007(4)	2.150(4)	1.984(3)	1.985(2)	1.984(3)	1.990(3)
Fe1…Fe1 _{inte^b}	8.468(1)	8.638(3)	8.807(4)	8.484(2)	8.562(2)	8.489(3)	8.492(3)
<i>Angle</i>							
N2–Fe1–N3	86.25(6)	85.75(14)	82.85(13)	86.26(10)	86.24(7)	86.17(10)	86.11(10)
N3–Fe1–N2a	93.75(6)	94.25(14)	97.15(13)	93.75(10)	93.76(7)	93.83(10)	93.89(10)
N1–Fe1–N1a	180	180	180	180	180	180	180
ΣFe^c	31	34	44	31	32	31	31
φ^d	25	40	64	37	38	37	40
$\pi\cdots\pi$ interactions ^a							
O1…C19g	3.199(3)	3.205(6)	3.221(8)	3.200(4)	3.207(4)	3.201(4)	3.203(5)
O1…C20g	3.076(2)	3.119(6)	3.138(7)	3.074(4)	3.105(3)	3.075(4)	3.076(5)
C15…C20g	3.323(2)	3.350(6)	3.348(7)	3.328(5)	3.335(3)	3.326(4)	3.333(5)
Cg6…Cg6b	4.589(1)	4.603(3)	4.623(4)	4.597(2)	4.600(2)	4.602(2)	4.614(2)
C8…C10p	3.555(2)	3.589(6)	3.605(3)	3.558(4)	3.583(3)	3.561(3)	3.562(5)
C7…C10p	3.654(2)	3.736(5)	3.762(3)	3.661(3)	3.713(3)	3.661(3)	3.666(5)
C9…N3p	3.700(2)	3.783(6)	3.806(2)	3.705(2)	3.753(3)	3.710(2)	3.711(4)
Cg4…Cg4p	3.682(1)	3.764(3)	3.786(3)	3.689(2)	3.739(1)	3.691(2)	3.692(2)
halogen…halogen contacts ^a							
F4…F7e	2.885(2)	2.933(5)	2.937(7)	2.883(3)	2.908(3)	2.885(3)	2.891(3)
F8…F9k	2.780(2)	2.852(5)	2.872(7)	2.783(3)	2.819(3)	2.777(3)	2.773(4)
Lone pair… π interactions ^a							
N7…F1c	3.104(2)	3.305(2)	3.268(7)	3.110(3)	3.144(3)	3.114(3)	3.127(4)
C12…F2c	3.014(2)	3.024(5)	3.047(7)	3.017(3)	3.015(3)	3.029(3)	3.041(4)
F1c…Cg5	3.238(2)	3.360(4)	3.478(5)	3.247(2)	3.313(2)	3.251(2)	3.258(3)

F2c···Cg5	3.443(2)	3.401(4)	3.398(5)	3.444(2)	3.415(2)	3.456(2)	3.468(3)
<i>Lone pair···π interactions^a</i>							
N1S···C21	3.202(3)	3.312(7)	3.332(10)	3.203(4)	3.276(4)	3.214(4)	3.225(5)
N1S···C26	3.278(3)	3.261(8)	3.320(11)	3.267(5)	3.252(4)	3.258(5)	3.255(6)
N1S···Cg7	3.413(2)	3.399(7)	3.466(10)	3.305(4)	3.367(4)	3.313(4)	3.321(5)
Se1···C22b	3.531(2)	3.663(5)	3.720(6)	3.539(3)	3.615(3)	3.544(3)	3.548(4)
Se1···C23b	3.772(2)	3.906(5)	3.935(5)	3.790(3)	3.850(3)	3.791(3)	3.797(4)
Se1···F6b	3.192(1)	3.239(3)	3.269(4)	3.191(2)	3.214(2)	3.187(2)	3.180(3)
Se1···Cg7	4.320(1)	4.486(3)	4.552(4)	4.337(2)	4.429(3)	4.345(2)	4.357(3)
Se1···C13	3.697(2)	3.755(4)	3.789(5)	3.707(3)	3.730(3)	3.713(3)	3.717(3)
Se1···Cg5	3.585(1)	3.654(2)	3.722(2)	3.595(1)	3.623(1)	3.600(1)	3.603(2)

^aSymmetry operations: a = 1-x, 1-y, 1-z; b = -1+x, y, z; c = 2-x, 1-y, 2-z; e = 2-x, 2-y, 2-z; g = 1-x, 1-y, 2-z; k = 2-x, 2-y, 1-z; p = 2-x, 1-y, 1-z.

^bClosest inter-monomer Fe···Fe distance (observed along the crystallographic *a* axis). ^cΣ = the sum of |90 - θ| for the 12 N–Fe–N angles in the octahedron.

^dΦ = sum of |60 - θ| for the 24 N–Fe–N angles describing the trigonal twist angle.

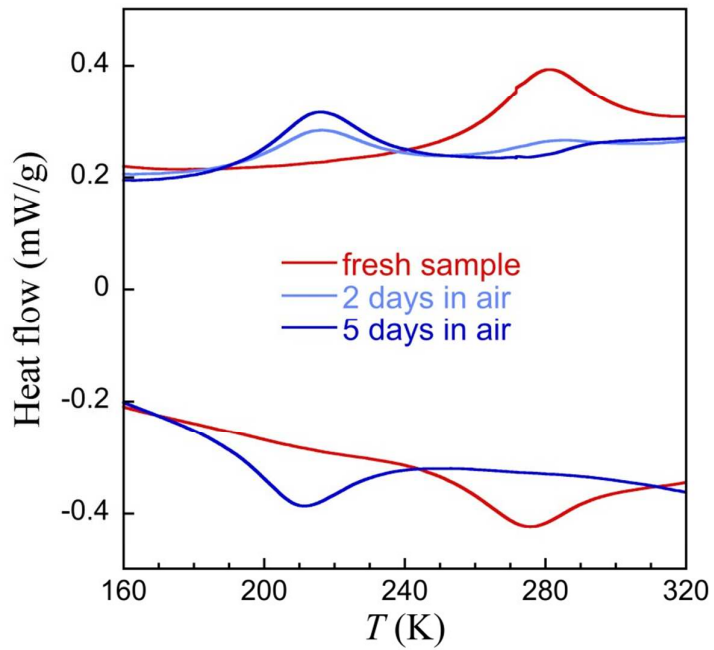


Figure S1. DSC traces (endotherms are up) of fresh $\mathbf{1}^{\text{NCSe}} \cdot \mathbf{2\text{PrCN}}$ (red lines) and of the same sample after respectively 2 (light blue lines) and 5 days (dark blue lines) in air. The latter is similar to that observed for the desolvated $\mathbf{1}^{\text{NCSe}}$ obtained by annealing $\mathbf{1}^{\text{NCSe}} \cdot \mathbf{2\text{PrCN}}$ for 2 hours at 80 °C.

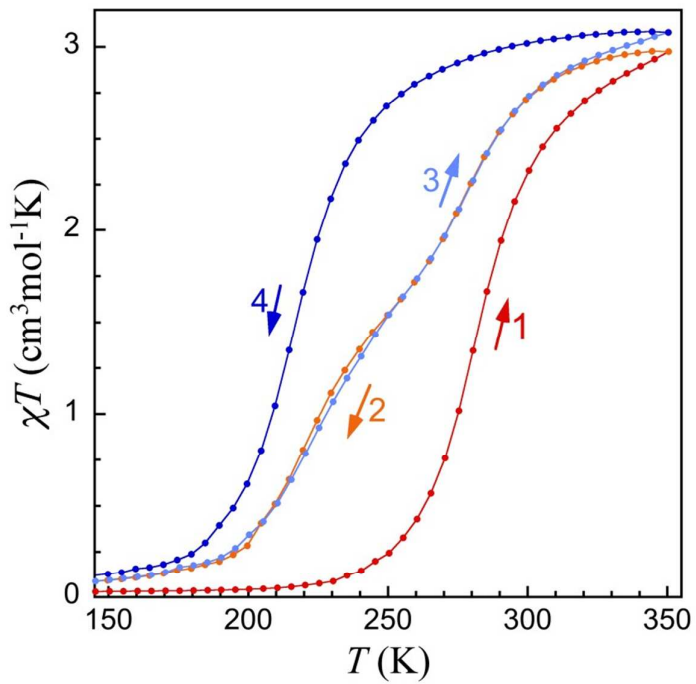


Figure S2. χT vs. T plots of four successive temperature scans, following the indicated sequence, starting with fresh **1^{NCSe}·2PrCN**. The sample was subjected to vacuum purges at RT before insertion, at 10 K, into the He depression environment of the magnetometer sample space. Further temperature scans did not show any further modification of the observed behavior.

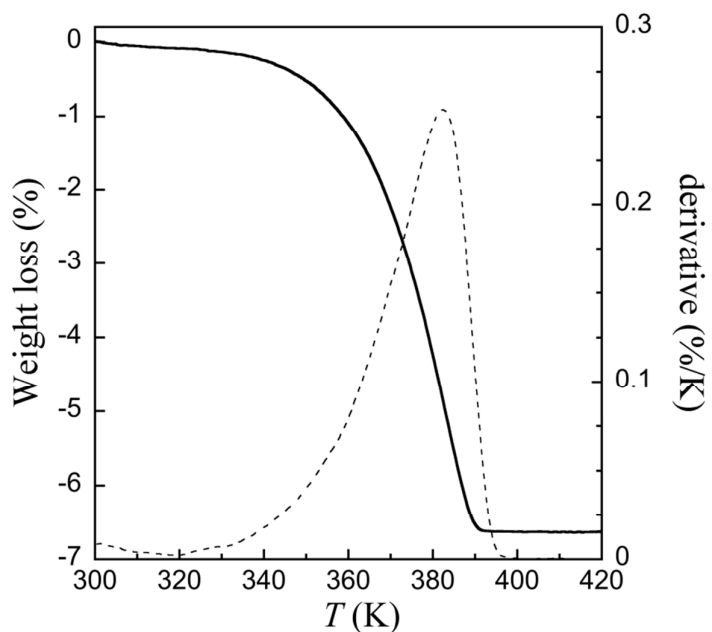


Figure S3. Thermogravimetric analysis of fresh $\mathbf{1}^{\text{NCSe}} \cdot \mathbf{2}\text{PrCN}$.

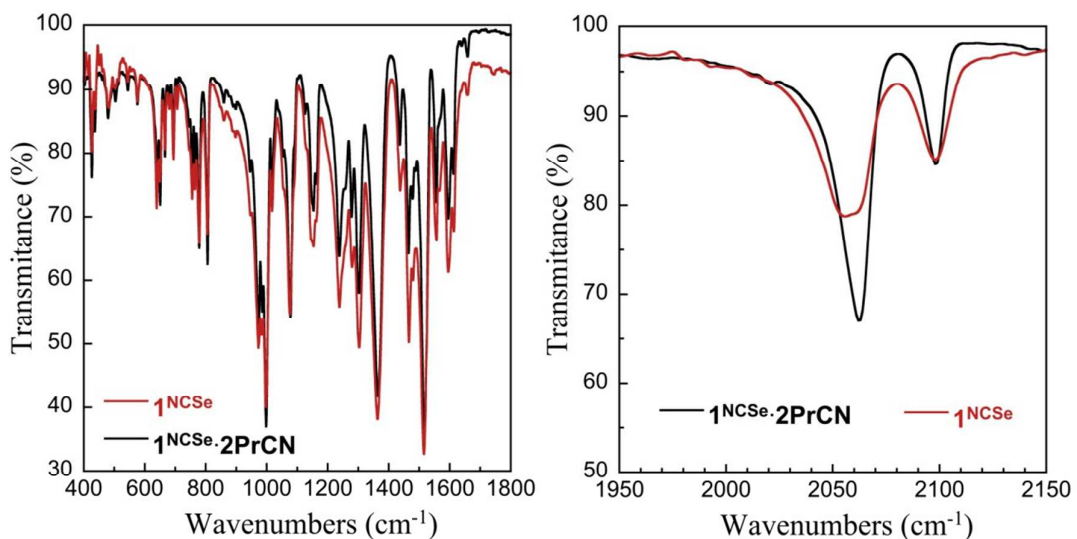


Figure S4. Comparison of the infra-red spectra (neat samples) of fresh $\mathbf{1}^{\text{NCSe}} \cdot \mathbf{2}\text{PrCN}$ (black lines) and $\mathbf{1}^{\text{NCSe}}$ (red lines), obtained by annealing the fresh material for 2 hours at 80 °C.

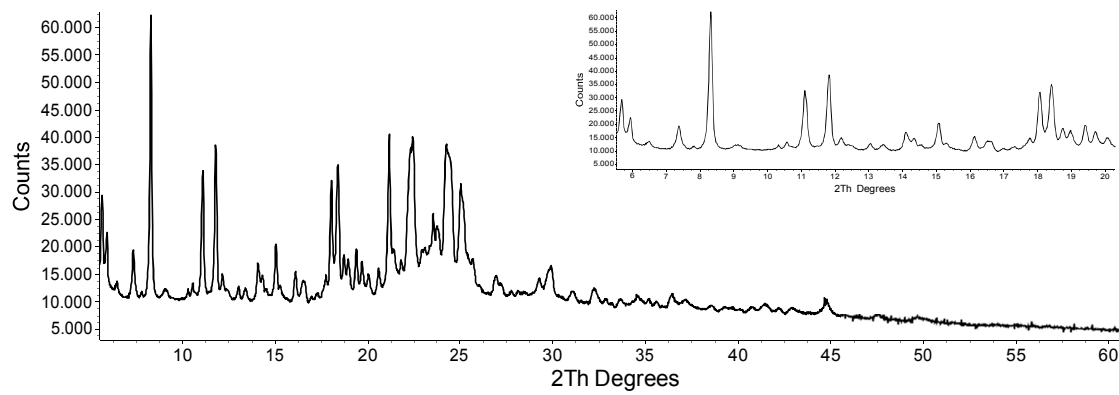


Figure S5. Raw diffraction data measured at room temperature for **1^{NCSe}**, after complete desolvation upon heating **1^{NCSe}·2PrCN** at 100 °C for ca. 1 h. The inset shows the low-angle region at an expanded scale.

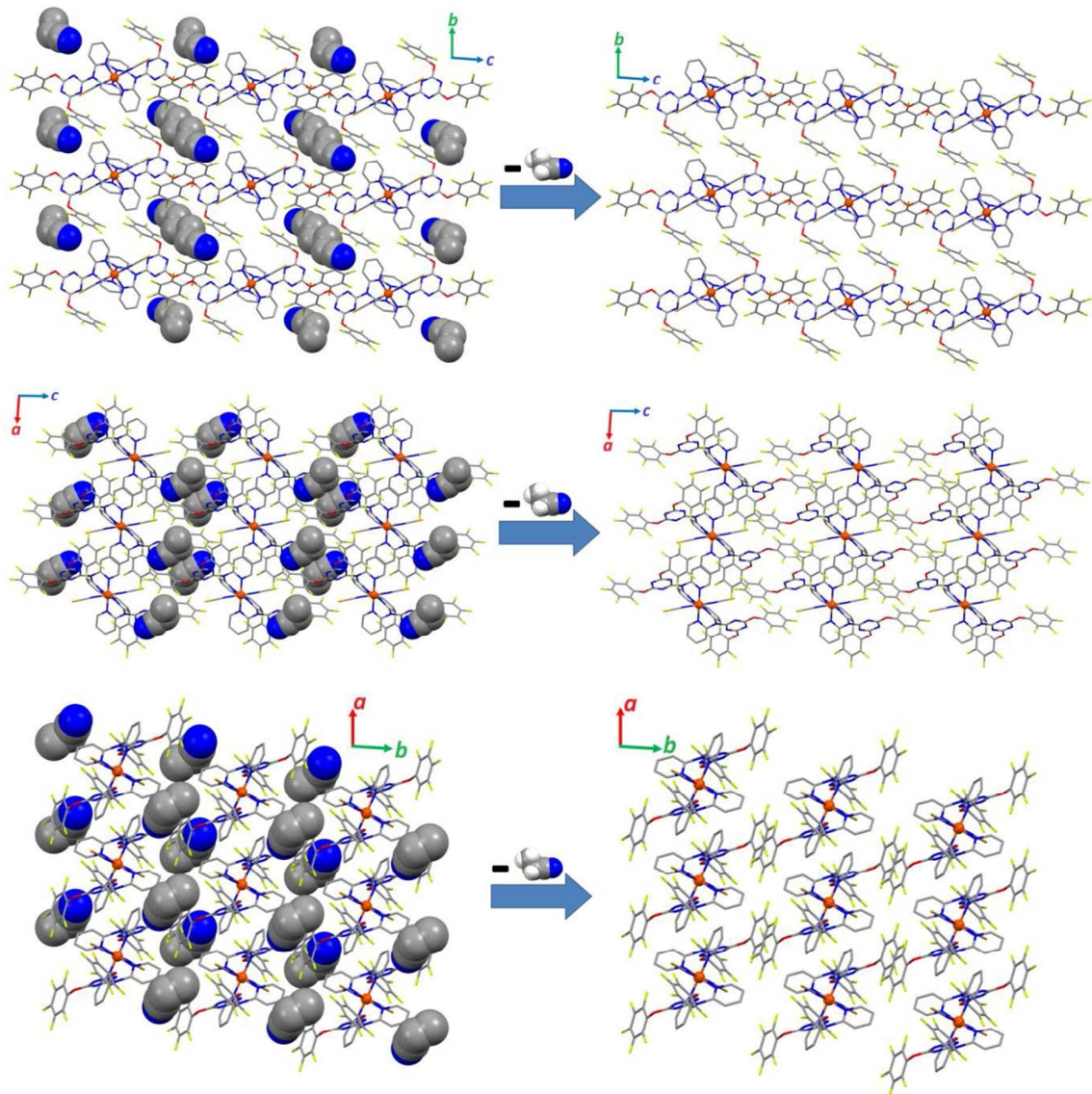


Figure S6. Views of the crystal packing of **1^{NCse}·2PrCN** in the *ab*, *bc* and *ac* planes showing the location of the propionitrile molecules in the lattice (left), and the voids generated upon their removal (right).